Strain-induced high-temperature perovskite ferromagnetic insulator

Dechao Meng[a,b,c,1], Hongli Guo[a,b,d,e,1], Zhangzhang Cui[a,b,c,f], Chao Ma[a,b], Jin Zhao[a,b,d,e], Jiangbo Lu[g], Hui Xu[a,b,c], Zhicheng Wang[a,b,c], Xiang Hu[a,b,c], Zhengping Fu[a,b], Ranran Peng[a,b], Jinghua Guo[f,h], Xiaofang Zhai[a,b,2], Gail J. Brown[i], Randy Knize[j], and Yalin Lu[a,b,c,i,j,2]

[a]Hefei National Laboratory for Physical Sciences at Microscale, University of Science and Technology of China, Hefei, 230026 Anhui, People's Republic of China; [b]Synergy Innovation Center of Quantum Information and Quantum Physics, University of Science and Technology of China, Hefei, 230026 Anhui, People's Republic of China; [c]National Synchrotron Radiation Laboratory, University of Science and Technology of China, Hefei, 230026 Anhui, People's Republic of China; [d]Key Laboratory of Strongly-Coupled Quantum Matter Physics, Chinese Academy of Sciences, University of Science and Technology of China, Hefei, 230026 Anhui, People's Republic of China; [e]Department of Physics, University of Science and Technology of China, Hefei, 230026 Anhui, People's Republic of China; [f]Advanced Light Source, Lawrence Berkeley National Laboratory, Berkeley, CA 94720; [g]School of Physics and Information Technology, Shaanxi Normal University, Xi'an, 710119 Shaanxi, People's Republic of China; [h]Department of Chemistry and Biochemistry, University of California, Santa Cruz, CA 95064; [i]Materials and Manufacturing Directorate, Air Force Research Laboratory, Wright-Patterson Air Force Base (AFB), Wright-Patterson AFB, OH 45433-7707; and [j]Laser Optics Research Center, US Air Force Academy, US Air Force Academy, CO 80840

Edited by Ivan Bozovic, Brookhaven National Laboratory, Upton, NY, and accepted by Editorial Board Member Zachary Fisk February 1, 2018 (received for review May 11, 2017)

Ferromagnetic insulators are required for many new magnetic devices, such as dissipationless quantum-spintronic devices, magnetic tunneling junctions, etc. Ferromagnetic insulators with a high Curie temperature and a high-symmetry structure are critical integration with common single-crystalline oxide films or substrates. So far, the commonly used ferromagnetic insulators mostly possess low-symmetry structures associated with a poor growth quality and widespread properties. The few known high-symmetry materials either have extremely low Curie temperatures (≤16 K), or require chemical doping of an otherwise antiferromagnetic matrix. Here we present compelling evidence that the $LaCoO_3$ single-crystalline thin film under tensile strain is a rare undoped perovskite ferromagnetic insulator with a remarkably high T_C of up to 90 K. Both experiments and first-principles calculations demonstrate tensile-strain–induced ferromagnetism which does not exist in bulk $LaCoO_3$. The ferromagnetism is strongest within a nearly stoichiometric structure, disappearing when the Co^{2+} defect concentration reaches about 10%. Significant impact of the research includes demonstration of a strain-induced high-temperature ferromagnetic insulator, successful elevation of the transition over the liquid-nitrogen temperature, and high potential for integration into large-area device fabrication processes.

ferromagnetic insulator | strain | defect | pulsed-laser deposition | X-ray absorption

The realization of a dopant-free ferromagnetic insulator (FMI) is critical to the fabrication of versatile spintronic devices due to the potential for dopants acting as undesirable inelastic scattering centers. In low-symmetry magnetic materials, an FMI may be realized through charge ordering in which magnetic ions occupy different atomic sites. Unfortunately, integrating such low-symmetry FMIs (1–4) into film devices presents significant challenges due to large lattice mismatch between the film and commonly used substrates, which almost universally possess high-symmetry structures. In high-symmetry structures, however, magnetic ions likely occupy identical crystallographic sites so that charge-ordering–stabilized FMI states are highly disfavored. Thus, undoped high-symmetry FMIs remain extremely rare (5–7). In fact, chemical doping has been always a prerequisite for making high-symmetry FMIs such as the colossal magnetoresistance oxides (8–12) and magnetic semiconductors (13, 14). The two well-known undoped high-symmetry FMIs, EuS and strained $EuTiO_3$, exhibit low Curie temperatures of about 16 and 4 K, respectively (5, 7). Therefore, engineering an undoped, FMI with high symmetry and high transition temperature (T_C) is highly desirable.

Normally, realizing an FMI requires a nonzero energy cost (ΔE) associated with electron hopping from an occupied metal orbital to a nearby unoccupied metal orbital through the bridging ligand orbital, so that the "hops" remain virtual events (15–17). Recently, the diamagnetic perovskite $LaCoO_3$ has been suggested as a possible high-symmetry FMI candidate due to the near-degeneracy of various spin states of the Co^{3+} ion, so that spin-state ordering may be readily achieved (18, 19). Such an ordering of the spin states, which may be induced through strain effects, was first theoretically proposed by Hsu et al. (20) and later by Demkov and coworkers (21) to explain the observed FM in the $LaCoO_3$ thin films (22, 23). However, previously fabricated $LaCoO_3$ thin films are susceptible to oxygen vacancy (O_v) ordering as observed in scanning transmission electron microscopy (STEM) studies (24–26). More recently, such O_v ordering was reported to be critical for the observed FM in nonstoichiometric $LaCoO_{3-\delta}$ films (25, 26). Currently, the nature of the FMI state in $LaCoO_3$ films remains unresolved, and the roles of strain and O_vs remains hotly debated. In addition to resolving these questions, it is critical to elucidate whether the $LaCoO_3$ film can in fact yield an

Significance

Ferromagnetic insulators are highly needed as the necessary components in developing next-generation dissipationless quantum-spintronic devices. Such materials are rare, and those high symmetric ones without chemical doping available so far only work below 16 K. Here we demonstrate a tensile-strained $LaCoO_3$ film to be a strain-induced high-temperature ferromagnetic insulator. Both experiments and first-principles calculations demonstrated that the tensile-strain–supported ferromagnetism reaches its strongest when the composition is nearly stoichiometric. It disappears when the Co^{2+} defect concentration reaches around 10%. The discovery represents a chance for the availability of such materials, a high operation temperature, and a high epitaxial integration potential for making future devices.

Author contributions: X.Z. and Y.L. designed research; D.M., H.G., Z.C., C.M., J.Z., J.L., H.X., Z.W., X.H., Z.F., R.P., J.G., X.Z., G.J.B., R.K., and Y.L. performed research; D.M., H.G., C.M., and X.Z. analyzed data; and X.Z. and Y.L. wrote the paper.

The authors declare no conflict of interest.

This article is a PNAS Direct Submission. I.B. is a guest editor invited by the Editorial Board.

[1]D.M. and H.G. contributed equally to this work.

[2]To whom correspondence may be addressed. Email: xfzhai@ustc.edu.cn or yllu@ustc.edu.cn.

This article contains supporting information online at www.pnas.org/lookup/suppl/doi:10.1073/pnas.1707817115/-/DCSupplemental.

Published online March 5, 2018.

undoped, high-temperature FMI with the high symmetry which enables high-quality growth.

In this work, we fabricated nearly stoichiometric $LaCoO_3$ films through pulsed-laser deposition under a maximal oxygen pressure of 25 Pa, which resulted in layer-by-layer growth. Details of the sample information can be found in *Materials and Methods* and *SI Appendix*, section I. We also fabricated various $LaCoO_3$ thin films in which the Co^{2+} concentration was systematically varied by tuning the oxygen pressure and film thickness. The latter increases the Co^{2+} defect density when the thickness is reduced below 10 unit cells (u.c.). Further experiments and first-principles calculations demonstrated that the film with minimal Co^{2+} under tensile strain exhibited the strongest FM state. The observed FM eventually disappears for Co^{2+} concentrations above ~10%. These results indicate that $LaCoO_3$ films under tensile strain may represent the unusual case of a high-symmetry undoped FMI with a T_C above liquid nitrogen temperature.

In Fig. 1*A*, we show magnetization and resistivity vs. temperature measurements for a 30-u.c. $LaCoO_3$ film grown under 25-Pa oxygen pressure on (001) $SrTiO_3$ substrate. The FM transition for this film appears at about 85 K. The resistivity increases with decreasing temperature from 390 to 70 K. Below 70 K, the resistance is over the measurement limit. A high-angle annular dark-field (HAADF) image, shown in Fig. 1*B*, was taken along the (010) direction by an aberration-corrected STEM. Long-range–ordered dark stripes associated with Co^{2+} state (25) or La–La elastic interactions (24) were not observed in either the present HAADF images or a variety of images taken in different areas and directions of the film, although we occasionally observed short, randomly distributed stripes in some areas (*SI Appendix*, section II). Co and Ti *L*-edge electron energy-loss spectroscopy (EELS), shown in Fig. 1*C*, reveals that the film–substrate interface is very sharp. Furthermore, the thickness oscillation fringes in the X-ray diffraction shown in Fig. 1*D* and the atomic force microscopy image in Fig. 1*E* both demonstrate the high quality of the fabricated $LaCoO_3$ film.

To further examine the nature of the observed FMI, we intentionally introduced controlled levels of oxygen vacancies into the film by reducing the oxygen growth pressure and by reducing the film thickness, yielding $LaCoO_{3-\delta}$ films. The corresponding reductions in T_C and magnetization are shown in Fig. 2*A*. We found that reducing the oxygen pressure causes T_C to decrease and a dramatic reduction occurs between 10 and 15 Pa. X-ray diffraction analyses in Fig. 2*B* show that by reducing the oxygen pressure the out-of-plane lattice constant increases dramatically, in agreement with a previous report (27). All films discussed in this paper are coherently strained to their substrates, either $SrTiO_3$ or $(LaAlO_3)_{0.3}(Sr_2TaAlO_6)_{0.7}$ (LSAT). We define an effective strain by $\varepsilon_{eff} = 1 - c/a$. In Fig. 2*C* the effective strain was found to match the T_C variation extremely well. Thus, reducing the oxygen pressure is associated with a reduction in T_C and magnetization which we attribute to a reduction in the effective tensile strain and increased nonstoichiometry.

Reducing the film thickness (at a constant growth pressure of 15 Pa) allows the T_C to be tuned more systematically while the effective strain remains relatively constant at ~3.5% in thicker films and ~3.3% in the 5-u.c. film. To probe the Co valence, we measured the Co *L*-edge and *K*-edge using soft X-ray absorption (XAS) and X-ray absorption near-edge structure (XANES) as shown in Fig. 2 *D* and *E*, respectively. In a $LaCoO_3$ film under tensile strain, Co^{3+} ions may exist in either the low-spin $t_{2g}^6e_g^0$ state (LS, $S = 0$) or the high-spin $t_{2g}^4e_g^2$ state (HS, $S = 2$) (19). The introduction of O_vs, however, could stabilize Co^{2+} HS states ($S = 1.5$) with an orbital occupancy of $t_{2g}^5e_g^2$ (26, 28, 29). Quantitative XAS spectral analysis using atomic multiplet plus the crystalline-field calculation (30, 31) was performed to extract the individual concentrations of the three spin states (more details in *SI Appendix*, section III). Additionally, the Co valence was quantitatively analyzed by comparing the measured XANES spectra to the reference spectra with a well-determined Co valence in a pseudocubic structure (32). The dependences of T_C and Co valence (both from the XAS and XANES) on the layer thickness are shown in Fig. 2*F*. Both decrease drastically as the thickness is reduced

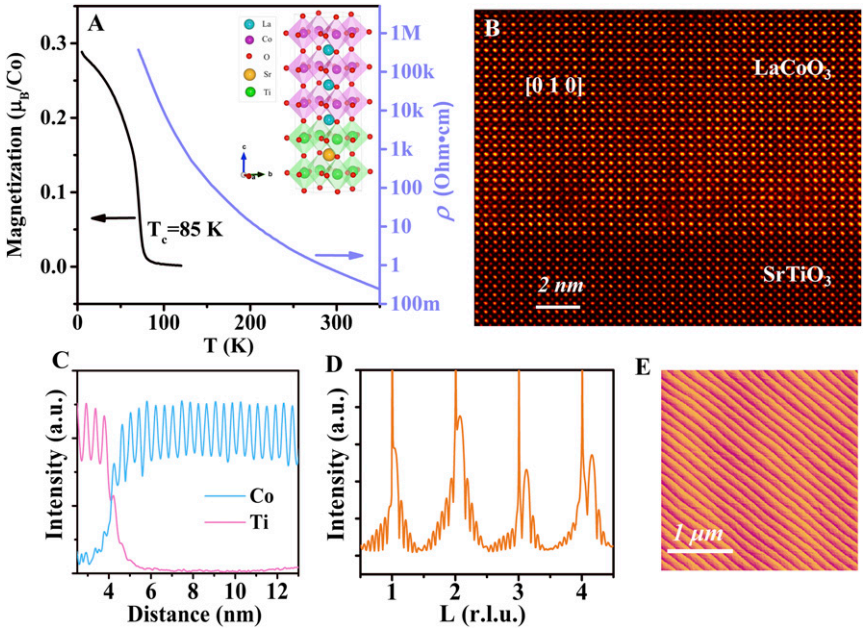

Fig. 1. FMI state in a nearly stoichiometric $LaCoO_3$ film under tensile strain. (*A*) Temperature dependences of the magnetization and resistivity of a 30-u.c. $LaCoO_3$ film grown on (001) $SrTiO_3$ at $p(O_2) = 25$ Pa. The magnetization was measured by a superconducting quantum interference device (SQUID) along the in-plane direction with a 500-Oe field after field cooling. (*Inset*) Schematic of the $LaCoO_3/SrTiO_3$ heterostructure. (*B*) Cross-section STEM-HAADF image of the film taken along the (010) direction. (*C*) Ti and Co layer-by-layer distributions across the interface measured by STEM-EELS. (*D*) Synchrotron XRD measurement of the (00L) peaks. (*E*) Atomically flat $LaCoO_3$ surface with terraces measured by atomic force microscopy.

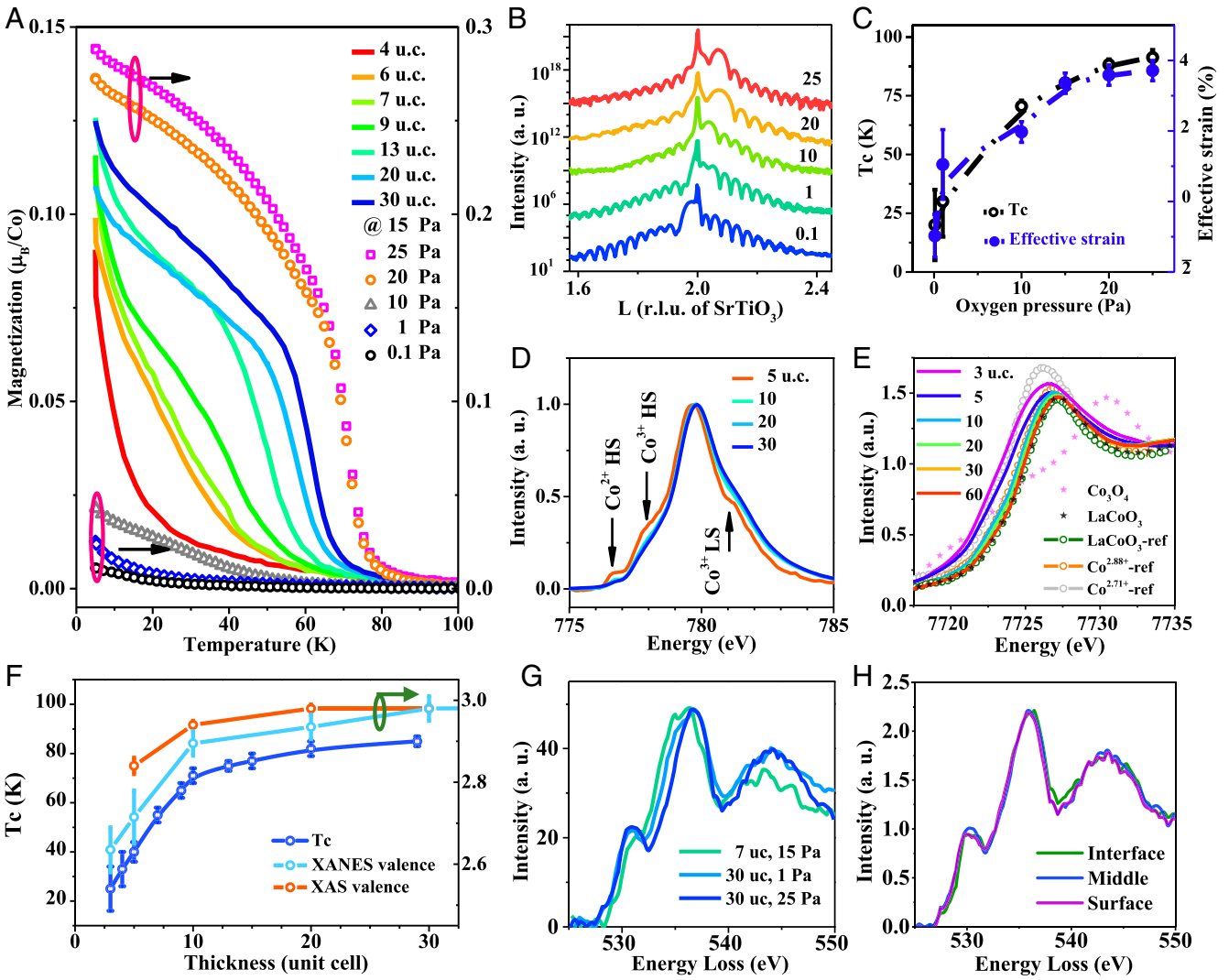

Fig. 2. Suppressed FM in $LaCoO_{3-\delta}$ films on $SrTiO_3$ substrates with released effective strain or with nonstoichiometry. (*A*) Temperature dependence of magnetization in $LaCoO_{3-\delta}$ films measured along the in-plane direction with a 500-Oe applied field after field cooling. (*B*) XRD scans of films grown with varied pressures. The fringes are total thickness oscillations indicating high-quality growth. (*C*) Dependences of T_C and effective strain on the growth pressure. (*D*) XAS spectra of films with varied thicknesses. (*E*) XANES spectra of films with varied thicknesses alongside reference spectra of bulk samples. Reprinted with permission from ref. 32, copyright (2006) by the American Physical Society. (*F*) Thickness dependences of T_C and Co valence measured by both XAS and XANES. (*G*) STEM-EELS oxygen *K*-edge spectra of three representative $LaCoO_3$ films. (*H*) EELS oxygen *K* edge of the three different blocks, each about 10 u.c., in the 30-u.c. nearly stoichiometric film.

below 10 u.c. The coincidence of T_C and Co valence transitions suggests that the introduced nonstoichiometry suppresses the FM.

Since the oxygen *K* edge is very sensitive to changes in the valence of the transition metal, we performed its STEM-EELS measurements to double check the Co valence obtained from XAS and XANES. We studied three representative samples on $SrTiO_3$ substrates (more details in *SI Appendix*, section II), including a thick film (30 u.c., 25 Pa), a thin film (7 u.c., 15 Pa), and a poorly oxygenated thick film (30 u.c., 1 Pa). The average oxygen *K*-edge spectra in Fig. 2*G* show that the 7-u.c. film exhibits a very weak preedge peak likely due to rich concentrations of O_v. From the line-by-line scans in the well-oxygenated 30-u.c. film, we do not observe clear trends of this prepeak weakening as the layer approaches the interface. To improve the signal quality and enable better comparison, we average the spectra of the top 10 layers, middle 10 layers, and interfacial 10 layers of the 30-u.c. films. We observe that the middle block has a slightly stronger prepeak than the surface and interfacial blocks, as shown in Fig. 2*H*.

To better understand the interplay between strain, off-stoichiometry, and FM in $LaCoO_3$ we performed first-principles density-functional theory (DFT) calculations, the details of which are shown in *Materials and Methods*. Consistent with previous investigations, the ground state of the strained $LaCoO_3$ is FM for $a = 3.905$ Å due to the high concentrations of HS Co^{3+} and FM coupling between the nearest HS and LS Co^{3+} (20, 21). Our calculations show that the FM in $LaCoO_3$ will indeed be suppressed by increasing the O_v density. Such O_vs introduce extra electrons which generate HS Co^{2+} atoms containing half-occupied e_g orbitals which support antiferromagnetic (AFM) superexchange between half-occupied orbitals, which decreases the magnetization. $LaCoO_3$ films with three different O_v concentrations were investigated using $2\sqrt{2}\times2\sqrt{2}\times4$ ($1O_v$/32Co), $2\sqrt{2}\times\sqrt{2}\times4$($1O_v$/16Co), and $2\sqrt{2}\times\sqrt{2}\times2$ ($1O_v$/8Co) u.c. (Fig. 3). Stoichiometric $LaCoO_3$ without O_v was also explored using three structural models discussed above, all yielding similar results. One can see that when the concentration is only $1O_v$/32Co (9.4% Co^{2+}), the magnetization only decreases slightly from 2 μ_B/Co to 1.6 μ_B/Co. This is because the AFM coupled HS Co^{2+} atoms

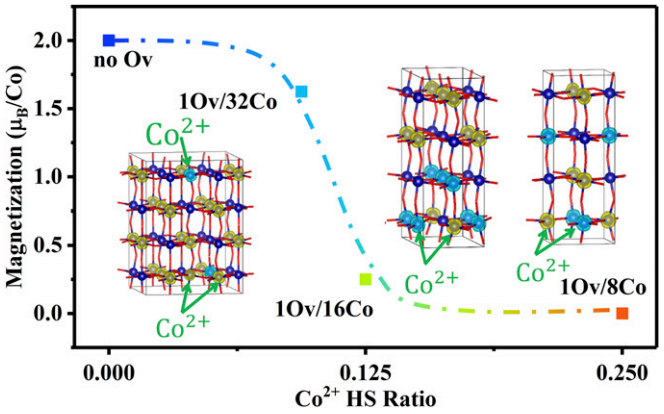

Fig. 3. Theoretically calculated magnetizations of the tensile-strained $LaCoO_{3-\delta}$ films with increased O_v concentrations. The three atomic pictures from left to right show the DFT calculated spin-state distribution in tensile-strained $LaCoO_{3-\delta}$ films of $1O_v$/32Co, $1O_v$/16Co, and $1O_v$/8Co, respectively. The atoms without density isosurface (blue colored) are LS Co^{3+}. The rest are HS Co^{3+} and HS Co^{2+}. The cyan- and yellow-colored isosurfaces have opposite spin directions.

only affect the local magnetic state. When the concentration increases to $1O_v$/16Co (12.5% Co^{2+}), the magnetization decreases dramatically to 0.2 μ_B/Co as the two Co^{2+} atoms introduce a long-range AFM coupling into the u.c. (more details in *SI Appendix*, section IV). For an even higher concentration of $1O_v$/8Co (25% Co^{2+}), the magnetization is close to zero. This behavior may be well described by a step function with an inflection point near a Co^{2+} concentration of 10%, in excellent agreement with our experimental results. The O_v-ordered $LaCoO_{3-\delta}$ thin films have been studied by Biškup et al. (25). Here we studied films with O_v concentrations much less than that of the previous work. Although details did not agree, both studies showed fewer magnetizations in O_v-occupied films than O_v-free films.

In addition to the studies of films on $SrTiO_3$ described above, we have performed similar experiments using $LaCoO_3$ films grown on (001) LSAT substrates with varied thicknesses, and found similar results. In Fig. 4, we summarize the T_C of all three thin-film groups, in addition to examples of films in the literature (23, 24, 26), as a function of effective strain and Co valence to create a phase diagram. Higher T_Cs are associated with the phase region with tensile strain and the lowest O_v concentrations. Away from this region, T_C is sharply reduced or the films are nonmagnetic. The universality and substrate-independent reproducibility of these trends supports the validity and generality of this study. Therefore, the experimental findings strongly suggest that tensile strain of nearly stoichiometric $LaCoO_3$ thin film results in a high-temperature FMI.

Relative to other examples of undoped high-symmetry FMIs, the $LaCoO_3$ Curie temperature is surprisingly high. A detailed understanding of this behavior is not yet clear and will require further exploration. One possible explanation is the larger overlap between the Co 3*d* and oxygen 2*p* orbitals. In other FMIs such as EuS, the FM originates in localized 4*f* electrons at the Eu sites and their orbital overlapping with the S 2*p* orbital or Eu 5*d* orbital (33, 34). On the other hand, our theoretical calculations show that the Co 3*d* orbital is much broader than the Eu 4*f* orbital and the superexchange interaction in $LaCoO_3$ films (21) is more than one order magnitude larger than that in the Eu chalcogenides (34). The availability of an undoped high-symmetry and high-T_C FMI is an important step toward bringing quantum-spintronic devices into the practical operation regime. Our results here indicate that the tensile-strained $LaCoO_3$ thin film is a much better technological candidate than previous low-temperature FMIs, thanks to the material's high T_C of nearly 90 K, its high cubic symmetry, and the ability to fabricate high-quality films over large areas on conventional substrates. The realization of such an FMI provides a solid foundation for the growth and design for next-generation device fabrication.

Materials and Methods

Sample Fabrication Using High-Pressure Reflective High-Energy Electron Diffraction Assisted Pulsed-Laser Deposition. Three groups of (001) $LaCoO_3$ thin films (summarized in *SI Appendix*, Table S1) were grown using a Pascal pulsed-laser deposition system assisted with double-differential pumped reflective high energy electron diffraction (RHEED). The $SrTiO_3$ substrates were etched in buffered hydrofluoric acid and annealed at 930 °C in flowing oxygen to obtain the uniform TiO_2 termination. All films were grown at 750 °C. The laser energy density was about 1.5 J/cm^2 and the frequency was 1 Hz. The thickness of $LaCoO_3$ films was precisely controlled by in situ RHEED oscillations, and later confirmed by ex situ X-ray reflectivity measurements. The lattice structures of films were measured by Synchrotron X-ray diffraction (XRD), carried out on BL14B1 (10 keV) at Shanghai Synchrotron Radiation Facility, 1W1A (10 keV) at Beijing Synchrotron Radiation Facility and 33-BM-C (22 keV) at Advanced Photon Source in Argonne National Laboratory.

XAS and XANES. Co *L*-edge XAS measurements were performed on BL6.3.1.2 at the Advanced Light Source of Lawrence Berkeley National Laboratory and BL12B-a at the National Synchrotron Radiation Laboratory of University of Science and Technology of China (USTC). XAS spectra were recorded in the total electron yield (TEY) and total fluorescence yield (TFY) mode simultaneously. The intensities were normalized to a reference signal recorded simultaneously on a gold mesh. The energy scale was calibrated by using metallic Co foil as reference. For the XAS TEY method, the penetration depth in the $LaCoO_3$ film was between 10 and 20 u.c. The measurements of Co *K*-edge XANES spectroscopy were carried out at room temperature at the beamline BL14W1 of the Shanghai Synchrotron Radiation Facility and 1W1B-XAFS of Beijing Synchrotron Radiation Facility. The signals were collected in the TFY mode at 45° with respect to the X-ray incident beam direction. Standard cobalt and iron metal foils were employed for energy calibration and fluorescence filtering, respectively. Each spectrum was collected at least three times to minimize the error.

First-Principles DFT Calculation. The electronic and magnetic properties of $LaCoO_3$ films on $SrTiO_3$ substrates with different amount of O_v were elucidated using first-principles DFT calculations, as implemented in Vienna Ab initio Simulation Package (VASP). The ion–electron interactions are described

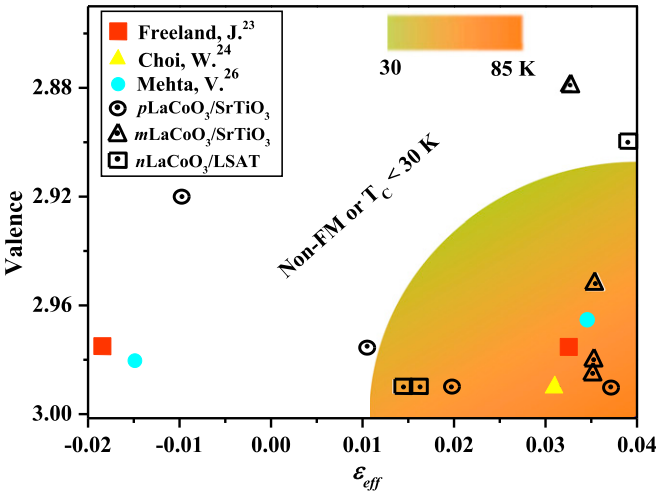

Fig. 4. Phase diagram of the FM T_C. The T_C, effective strain ε_{eff}, and Co valence are all from experimental results. In the white-colored region, T_C is below 30 K and is difficult to be quantified due to the paramagnetic background in SQUID measurements. Open circles, triangles, and squares with dots inside represent the three series of samples fabricated in this study (*SI Appendix*, Table S1). The *p* series refer to the varying pressure films on $SrTiO_3$. *m* and *n* series refer to the varying thickness films on $SrTiO_3$ and LSAT, respectively. Solid-color symbols represent films from the literature (23, 24, 26).

by the projector-augmented wave method. We use the generalized gradient approximation (GGA) with PW91 functional. Static local electronic correlations are added to the GGA exchange-correlation potential in the GGA+U method with $U = 5.27$ eV and $J = 1.47$ eV (Co_{3d}) as Seo et al. (21) did. In our calculations, all of the atomic positions are relaxed until the force on each atom is less than 0.01 eV/Å, and all of the self-consistent electronic calculations are converged to 10^{-6} eV per cell. To study the O_v effect on the magnetic solution in $LaCoO_3$ film on $SrTiO_3$, $2\sqrt{2}\times\sqrt{2}\times2$, $2\sqrt{2}\times\sqrt{2}\times4$, and $2\sqrt{2}\times2\sqrt{2}\times4$ supercells were used by introducing one O_v per supercell. We used the experimental lattice constant of $SrTiO_3$ $a = 3.905$ Å to fix the in-plane lattice constant of the $LaCoO_3$ film. With this lattice constant, a 3.5% tensile strain is applied to the $LaCoO_3$ film.

STEM. Specimens for STEM characterization were prepared by focused ion beam along the pseudocubic (010) direction of films on $SrTiO_3$ substrates. Specimens along (100, 110, 1-10) directions of the 30-u.c film on $SrTiO_3$ substrate grown with $P(O_2) = 25$ Pa were also measured which are also absent of long-range O_v order. Spherical-aberration–corrected HAADF images were acquired on a JEOL ARM200F microscope operating at 200 kV. For HAADF images, the convergence angle was about 23 mrad, and the inner and outer angles of the detectors was 90 and 370 mrad, respectively. The experimental STEM images were low-pass filtered. The intensity of every atomic column in the HAADF images was approximately proportional to $Z^{1.7}$ (Z is the atomic number).

ACKNOWLEDGMENTS. We thank Dr. Alexander J. Grutter for helpful discussions and manuscript editing. This work was partially carried out at the USTC Center for Micro and Nanoscale Research and Fabrication. This work was supported by the National Natural Science Foundation of China (Grants 51627901, 11574287, 21373190, 11620101003, and 11574281), the National Key Research and Development Program of China (Grant 2016YFA0401004), Open Programs for the Key Science & Technology Infrastructures of Chinese Academy of Sciences, Youth Innovation Promotion Association Chinese Academy of Sciences (Grant 2016389), and the Fundamental Research Funds for the Central Universities (Grant WK2340000065). This research used resources of the Advanced Light Source, which is a Department of Energy Office of Science User Facility under Contract DE-AC02-05CH11231.

1. Ziolo RF, et al. (1992) Matrix-mediated synthesis of nanocrystalline γ-Fe_2O_3: A new optically transparent magnetic material. *Science* 257:219–223.
2. Emori S, et al. (2017) Coexistence of low damping and strong magnetoelastic coupling in epitaxial spinel ferrite thin films. *Adv Mater* 29:1701130.
3. Mahadevan P, Kumar A, Choudhury D, Sarma DD (2010) Charge ordering induced ferromagnetic insulator: $K_2Cr_8O_{16}$. *Phys Rev Lett* 104:256401.
4. Christianson AD, et al. (2008) Three-dimensional magnetic correlations in multiferroic $LuFe_2O_4$. *Phys Rev Lett* 100:107601.
5. Mauger A, Godart C (1986) The magnetic, optical, and transport properties of representatives of a class of magnetic semiconductors: The europium chalcogenides. *Phys Rep* 141:51–176.
6. Katmis F, et al. (2016) A high-temperature ferromagnetic topological insulating phase by proximity coupling. *Nature* 533:513–516.
7. Lee JH, et al. (2010) A strong ferroelectric ferromagnet created by means of spin-lattice coupling. *Nature* 466:954–958.
8. Zener C (1951) Interaction between the d shells in the transition metals. *Phys Rev* 81: 440–444.
9. Anderson PW (1955) Considerations on double exchange. *Phys Rev* 100:675–681.
10. De Gennes PG (1960) Effects of double exchange in magnetic crystals. *Phys Rev* 118: 141–154.
11. Schiffer P, Ramirez AP, Bao W, Cheong SW (1995) Low temperature magnetoresistance and the magnetic phase diagram of $La_{1-x}Ca_xMnO_3$. *Phys Rev Lett* 75:3336–3339.
12. Ruderman M, Kittel C (1954) Indirect exchange coupling of nuclear magnetic moments by conduction electrons. *Phys Rev* 96:99–102.
13. Ohno H (1998) Making nonmagnetic semiconductors ferromagnetic. *Science* 281: 951–955.
14. Matsumoto Y, et al. (2001) Room-temperature ferromagnetism in transparent transition metal-doped titanium dioxide. *Science* 291:854–856.
15. Anderson PW (1950) Antiferromagnetism. Theory of superexchange interaction. *Phys Rev* 79:350–356.
16. Goodenough JK (1958) An interpretation of the magnetic properties of the perovskite-type mixed crystals $La_{1-x}Sr_xCoO_{3-\lambda}$. *J Phys Chem Solids* 6:287–297.
17. Kanamori J (1959) Superexchange interaction and symmetry properties of electron orbitals. *J Phys Chem Solids* 10:87–98.
18. Korotin MA, et al. (1996) Intermediate-spin state and properties of $LaCoO_3$. *Phys Rev B Condens Matter* 54:5309–5316.
19. Haverkort MW, et al. (2006) Spin state transition in $LaCoO_3$ studied using soft x-ray absorption spectroscopy and magnetic circular dichroism. *Phys Rev Lett* 97:176405.
20. Hsu H, Blaha P, Wentzcovitch R (2012) Ferromagnetic insulating state in tensile-strained $LaCoO_3$ thin films from LDA+U calculations. *Phys Rev B* 85:140404.
21. Seo H, Posadas A, Demkov A (2012) Strain-driven spin-state transition and superexchange interaction in $LaCoO_3$: Ab initio study. *Phys Rev B* 86:014430.
22. Fuchs D, et al. (2007) Ferromagnetic order in epitaxially strained $LaCoO_3$ thin films. *Phys Rev B* 75:144402.
23. Freeland J, Ma J, Shi J (2008) Ferromagnetic spin-correlations in strained $LaCoO_3$ thin films. *Appl Phys Lett* 93:212501.
24. Choi WS, et al. (2012) Strain-induced spin states in atomically ordered cobaltites. *Nano Lett* 12:4966–4970.
25. Biškup N, et al. (2014) Insulating ferromagnetic $LaCoO_{3-\delta}$ films: A phase induced by ordering of oxygen vacancies. *Phys Rev Lett* 112:087202.
26. Mehta V, et al. (2015) Long-range ferromagnetic order in $LaCoO_{3-\delta}$ epitaxial films due to the interplay of epitaxial strain and oxygen vacancy ordering. *Phys Rev B* 91: 144418.
27. Mehta V, Suzuki Y (2011) Ferromagnetism enhanced by structural relaxation of biaxially compressed LaCoO3 films. *J Appl Phys* 109:07D717.
28. Pinta C, et al. (2008) Suppression of spin-state transition in epitaxially strained $LaCoO_3$. *Phys Rev B* 78:174402.
29. Merz M, et al. (2010) X-ray absorption and magnetic circular dichroism of $LaCoO_3$, $La_{0.7}Ce_{0.3}CoO_3$, and $La_{0.7}Sr_{0.3}CoO_3$ films: Evidence for cobalt-valence-dependent magnetism. *Phys Rev B* 82:174416.
30. de Groot FM, Fuggle JC, Thole BT, Sawatzky GA (1990) 2*p* x-ray absorption of 3d transition-metal compounds: An atomic multiplet description including the crystal field. *Phys Rev B Condens Matter* 42:5459–5468.
31. De Groot F (2005) Multiplet effects in X-ray spectroscopy. *Coord Chem Rev* 249:31–63.
32. Sikora M, et al. (2006) X-ray absorption near-edge spectroscopy study of Mn and Co valence states in $LaMn_{1-x}Co_xO_3$ (x=0–1). *Phys Rev B* 73:094426.
33. McGuire TR, Shafer MW (1964) Ferromagnetic europium compounds. *J Appl Phys* 35: 984–988.
34. Kuneš J, Ku W, Pickett W (2005) Exchange coupling in Eu monochalcogenides from first principles. *J Phys Soc Jpn* 74:1408–1411.